Research Square

Preprints are preliminary reports that have not undergone peer review.
They should not be considered conclusive, used to inform clinical practice,
or referenced by the media as validated information.

Adipose-Derived Stem Cell Sheets Enhance Diced Cartilage Graft Survival via Regulation of the Autophagy–Pyroptosis Axis

Yi Wei
First Affiliated Hospital of University of South China
Tianjing Yu
First Affiliated Hospital of University of South China
Zhengyang Li
First Affiliated Hospital of University of South China
Wencan Li
First Affiliated Hospital of University of South China
Yan Chen
First Affiliated Hospital of University of South China
Can Liu
Third Xiangya Hospital
Li Li
First Affiliated Hospital of University of South China
Jianda Zhou
Third Xiangya Hospital
Junlin Liao
liaojunlin85@163.com

First Affiliated Hospital of University of South China

Research Article

Keywords: Diced Cartilage, ADSCs Sheet, Transplant Microenvironment, Cartilage Regeneration, Pyroptosis

Posted Date: July 28th, 2026

DOI: https://doi.org/10.21203/rs.3.rs-9687934/v1

License: This work is licensed under a Creative Commons Attribution 4.0 International License.
Read Full License

Additional Declarations: No competing interests reported.

Abstract

Background

Autologous diced costal cartilage is widely used in rhinoplasty and auricular reconstruction; however, long-term graft survival is often compromised by oxidative stress, inflammation, and insufficient vascularization after transplantation. Emerging evidence suggests that NLRP3/Caspase-1/GSDMD-mediated pyroptosis and impaired autophagy contribute to chondrocyte injury and cartilage degeneration. This study investigated whether adipose-derived stem cell (ADSC) sheets could improve diced cartilage graft survival by regulating the autophagy–pyroptosis axis.

Methods

A rabbit ectopic transplantation model was established to evaluate the effects of ADSC sheet wrapping on diced cartilage grafts in vivo. Histological staining, TUNEL assay, immunohistochemistry, and immunofluorescence were performed to assess graft morphology, apoptosis, oxidative stress, pyroptosis, and autophagy. In vitro, human chondrocytes were exposed to H_2O_2-induced oxidative stress and co-cultured with ADSCs. Cell viability, reactive oxygen species (ROS), migration, inflammatory cytokines, and related molecular markers were analyzed by CCK-8, flow cytometry, RT-qPCR, western blotting, ELISA, and transmission electron microscopy. Autophagy was modulated using rapamycin and bafilomycin A1. Statistical analyses were performed using Student's t-test or one-way ANOVA.

Results

ADSC sheet-wrapped grafts showed improved cartilage architecture, increased retention of chondrocyte lacunae, reduced apoptosis and nuclear loss, and enhanced type II collagen deposition compared with control and autologous perichondrium groups. ADSC sheets significantly suppressed NLRP3, Caspase-1, GSDMD, and NOX4 expression, while increasing SOD1, LC3, and Beclin-1 and decreasing P62, indicating reduced oxidative stress, inhibited pyroptosis, and enhanced autophagy. In vitro, ADSCs attenuated H_2O_2-induced oxidative stress, reduced ROS accumulation and inflammatory cytokine secretion, restored autophagic flux, and suppressed pyroptosis in chondrocytes. Rapamycin further enhanced these protective effects, whereas bafilomycin A1 partially reversed them. Transcriptomic analysis further confirmed coordinated regulation of autophagy-, inflammation-, and metabolism-related pathways.

Conclusions

ADSC sheets function as a biomimetic regenerative niche that improves the transplantation microenvironment and enhances diced cartilage graft survival by promoting autophagy and suppressing NLRP3/Caspase-1/GSDMD-mediated pyroptosis. This strategy provides a promising stem cell-based approach for improving long-term cartilage graft stability in reconstructive surgery.

1.Introduction

Cartilage transplantation is widely used in reconstructive and aesthetic surgery to restore structural integrity and function in craniofacial and orthopedic defects. Compared with synthetic implants such as silicone, expanded polytetrafluoroethylene, or porous polyethylene, autologous cartilage exhibits superior biocompatibility, structural stability, and minimal risk of immune rejection or extrusion [1]. Among various grafting approaches, autologous diced cartilage—generated by cutting septal, auricular, or costal cartilage into particles of approximately 0.5–1.0 mm^3—has attracted increasing attention due to its flexible shaping capability, favorable tissue compatibility, and reduced graft visibility [2,3]. Since its first clinical application reported by William A. Peer in 1945, diced cartilage has been widely applied in procedures such as rhinoplasty and auricular reconstruction [4]. Recent studies further indicate that diced cartilage grafts may exhibit higher chondrocyte survival rates than block or sheet cartilage grafts [5]. Despite these advantages, the long-term survival of diced cartilage grafts remains limited by the unfavorable transplantation microenvironment. Because cartilage is an avascular and aneural tissue, transplanted grafts lack direct vascular supply and are therefore susceptible to oxidative stress, inflammatory responses, and metabolic imbalance after implantation [6]. These factors impair chondrocyte viability and accelerate extracellular matrix degradation, ultimately leading to cartilage resorption. Clinical analyses have reported measurable rates of postoperative graft resorption in autologous cartilage transplantation, highlighting the need for strategies that stabilize the graft microenvironment and preserve chondrocyte viability [7].

Wrapping techniques using autologous perichondrium or fascia have been employed to provide mechanical support and a relatively protective microenvironment for diced cartilage grafts, thereby promoting neovascularization and reducing inflammation [8,9]. However, their clinical use is limited by donor tissue availability and potential donor-site morbidity. Cell sheet technology has recently emerged as a promising biomimetic strategy. By preserving intact cell–cell junctions and extracellular matrix components, cell sheets facilitate cell survival, engraftment, and functional integration [10–12]. Adipose-derived stem cells (ADSCs), a major component of stromal vascular fractions (SVFs), possess strong paracrine, immunomodulatory, and regenerative capacities [13]. Previous studies have shown that ADSCs can enhance extracellular matrix synthesis and suppress inflammatory responses in cartilage tissues [14]. Our previous work further demonstrated that SVFs improve vascularization and survival of diced cartilage grafts, and that SVF-derived cell sheets promote graft survival more effectively than direct cell injection, although the underlying mechanisms remain unclear [15].

Recent evidence suggests that chondrocyte pyroptosis—an inflammatory form of programmed cell death mediated by gasdermin proteins—plays a key role in cartilage degeneration [16,17]. Pyroptosis is characterized by membrane rupture and release of proinflammatory cytokines such as interleukin-1β (IL-1β), thereby amplifying inflammatory responses [18]. This process has been implicated in degenerative cartilage diseases, including osteoarthritis and intervertebral disc degeneration [19–21]. Oxidative stress is considered a major upstream trigger, as excessive reactive oxygen species (ROS) disrupt redox homeostasis, induce mitochondrial dysfunction, and promote inflammatory signaling [22–24]. Autophagy, a

lysosome-dependent degradation pathway responsible for recycling damaged organelles and proteins, is an important mechanism for maintaining cellular homeostasis under stress [25,26]. Emerging evidence indicates a complex interaction between autophagy and pyroptosis: moderate autophagy activation may suppress pyroptosis by removing damaged mitochondria, whereas dysregulated autophagy may exacerbate cellular injury [27–29]. Although ADSCs have been reported to inhibit pyroptosis-related signaling and attenuate inflammation in cartilage degeneration models, whether similar mechanisms operate in diced cartilage transplantation remains unknown [30]. In particular, it is unclear whether ADSC-derived cell sheets can regulate oxidative stress, autophagy, and pyroptosis in transplanted chondrocytes, thereby improving graft survival.

In this study, an ectopic autologous diced cartilage transplantation model was established in New Zealand white rabbits to evaluate the effects of ADSC cell sheet wrapping on graft survival. In parallel, a hydrogen peroxide (H_2O_2)-induced oxidative stress model of human chondrocytes was constructed in vitro to investigate the regulatory roles of ADSCs in pyroptosis, oxidative stress, and autophagy. Autophagy modulation experiments were further performed to clarify its involvement in this process. This study aims to elucidate the cellular mechanisms underlying ADSC-mediated protection of cartilage grafts and to provide experimental evidence for improving cartilage graft survival using cell sheet–based strategies.

2. Material and methods

2.1. Animals

Eighteen 6-month-old New Zealand White rabbits (2.3–2.5 kg, both sexes) were obtained from the Animal Center of the University of South China (License No. SYXK (Xiang) 2020-0002). Animals were housed individually under controlled conditions (24°C, 50%–60% humidity, 12 h light/dark cycle) with free access to standard chow and water for 1 week prior to surgery. All experimental procedures were approved by the Experimental Animal Ethics Committee of the University of South China and conducted in accordance with institutional and national guidelines for the care and use of laboratory animals. Rabbits were anesthetized by intravenous injection of 25% urethane (4 mL/kg) via the marginal ear vein. Local infiltration anesthesia was subsequently performed using 5% lidocaine at the auricular root. Surgical procedures were initiated only after an adequate depth of anesthesia had been confirmed by the absence of pedal withdrawal and corneal reflexes. One ear was surgically resected under sterile conditions. Auricular cartilage was harvested, and the surrounding soft tissues, including skin, fascia, and perichondrium, were carefully removed. The cartilage was minced into approximately 0.5–1.0 mm^3 particles and randomly divided into three groups: (i) unwrapped diced cartilage (control group), (ii) diced cartilage wrapped with autologous fascia (autologous membrane group), and (iii) diced cartilage wrapped with preformed ADSC sheets (ADSC sheet group). Three separate subcutaneous pockets were created on the dorsal region of each rabbit, and the corresponding grafts were implanted individually. The incisions were then closed with sutures. Postoperatively, rabbits received intramuscular penicillin (4

× 10^5 U immediately after surgery and once daily for 3 consecutive days). Animals were monitored daily for wound healing, general health, and food intake. At 1, 3, and 6 months after implantation (n = 6 per time point), rabbits were humanely euthanized by intravenous administration of an overdose of sodium pentobarbital (150 mg/kg) via the marginal ear vein. Death was confirmed by the absence of heartbeat and spontaneous respiration before graft harvesting. The harvested specimens were subsequently subjected to macroscopic evaluation, hematoxylin–eosin staining, TUNEL assay, and immunohistochemical analysis.

2.2. Isolation and culture of rabbit adipose-derived stem cells

Adipose-derived stem cells (ADSCs) were isolated from inguinal adipose tissue of New Zealand White rabbits under sterile conditions. Prior to surgery, rabbits were fasted for at least 6 h and anesthetized via ear vein injection of 25% urethane (4 mL kg^{-1}). After routine skin preparation and aseptic draping, a 2–3 cm incision was made in the inguinal region, and approximately 5 mL of subcutaneous adipose tissue was carefully harvested while avoiding neurovascular injury. Hemostasis was achieved, and the incision was closed in layers using 4 – 0 silk sutures. Postoperative monitoring included daily wound inspection and suture removal at day 7. Collected adipose tissue was rinsed twice with phosphate-buffered saline (PBS) to remove blood and debris, minced into small fragments, and digested in 1 mg mL^{-1} trypsin at 37°C for 1 h with gentle agitation. Enzymatic digestion was terminated by adding an equal volume of high-glucose Dulbecco's modified Eagle's medium (DMEM) supplemented with 10% fetal bovine serum (FBS) and 1% penicillin–streptomycin. The cell suspension was filtered through a sterile mesh to remove undigested tissue and centrifuged at 1500 rpm for 10 min. The stromal vascular fraction was collected, resuspended in mesenchymal stem cell medium (MSCM) containing 10% FBS, and seeded into 100 mm culture dishes at a density of 1 × 10^5 cells mL^{-1} (10 mL per dish). Cells were maintained at 37°C in a humidified atmosphere with 5% CO_2, with medium changes every 2–3 d. Passage was performed upon reaching 80%–90% confluence.

2.3. Characterization of ADSCs and preparation of ADSC sheets

Second-passage (P2) rabbit ADSCs were characterized prior to subsequent applications. Cellular morphology was examined under phase-contrast microscopy. For immunophenotypic analysis, cells were detached with 0.35% trypsin, centrifuged at 1000 r min^{-1} for 5 min, washed once with PBS, and resuspended at a density of 1 × 10^6 cells mL^{-1}. The cell suspension was incubated with rabbit monoclonal antibodies against CD34, CD45, CD73, CD90, and CD105 (20 µL each) for 15 min at room temperature in the dark, followed by flow cytometric analysis. For ADSC sheet fabrication, P2 cells were seeded onto 3.5 cm temperature-responsive culture dishes at a density of 1 × 10^6 cells cm^{-2} and cultured in L-DMEM supplemented with 10% fetal bovine serum at 37°C in a humidified atmosphere containing 5% CO_2. Upon reaching approximately 90% confluence, the medium was replaced with sheet-induction medium consisting of L-DMEM supplemented with 10% fetal bovine serum, 50 µg mL^{-1} vitamin C, and

1% penicillin–streptomycin. The medium was refreshed daily for 14 d to promote extracellular matrix deposition and sheet formation. Mature cell sheets were harvested by incubating the dishes at 20°C for approximately 40 min, allowing spontaneous detachment from the temperature-responsive surface and yielding intact ADSC sheets for subsequent experiments.

2.4. Ultrastructural observation of ADSC sheets

The ultrastructure of ADSC sheets was examined by electron microscopy. Freshly prepared sheets were immediately fixed in pre-cooled 2.5% glutaraldehyde at 4°C in the dark, followed by rinsing with phosphate buffer four times (1 h each). Samples were post-fixed in 1% osmium tetroxide at 4°C for 2 h and washed three times with double-distilled water (10 min each). Subsequently, specimens were stained en bloc with 2% aqueous uranyl acetate for 2 h and dehydrated through a graded ethanol series (50%, 70%, 90%, and 100%; 15 min each), followed by two changes of absolute acetone (20 min each). Samples were then infiltrated with a 1:1 mixture of 100% acetone and embedding resin for 2 h at room temperature. After embedding and polymerization, ultrathin sections were prepared, stained with lead citrate, air-dried, and observed under an electron microscope.

2.5. Histological analysis by hematoxylin–eosin (H&E) staining

Harvested diced cartilage grafts were trimmed into approximately 5 mm × 5 mm × 3 mm specimens and fixed in 4% paraformaldehyde for 48 h, followed by rinsing in running water. Samples were dehydrated through a graded ethanol series (70%, 80%, 90%, and 95%, 1 h each; absolute ethanol for 30 min), cleared in ethanol/xylene (1:1) and xylene I and II (20 min each), and infiltrated with molten paraffin at 60°C (1 h, repeated twice). Tissues were then embedded in paraffin, sectioned at ~ 10 μm thickness, mounted onto glass slides, and dried at 40°C for 1.5 h. For staining, sections were deparaffinized in xylene (20 min × 3) and rehydrated through graded ethanol (100%, 95%, 85%, and 75%, 5 min each) to distilled water. Slides were stained with hematoxylin for 5 min, differentiated in 1% acid alcohol for 5 s, blued in 1% ammonia water for 10 s, and rinsed thoroughly. Subsequently, sections were counterstained with eosin for 5 min after dehydration in 85% and 95% ethanol (5 min each). Finally, sections were dehydrated in graded ethanol (95%–100%), cleared in xylene (10 min × 2), sealed with neutral resin, and observed under a light microscope.

2.6. TUNEL assay

Apoptotic cells within paraffin-embedded diced cartilage sections were detected using a TUNEL assay according to the manufacturer's instructions. Briefly, sections were deparaffinized in xylene (10 min × 2), rehydrated through graded ethanol (100%, 95%, 85%, and 75%, 5 min each), and rinsed in distilled water. Sections were incubated with freshly prepared Proteinase K working solution (1 μL 100× Proteinase K in 99 μL 1× PBS per sample; 100 μL/section) at 37°C for 20 min, followed by washing in PBS (5 min × 3). After equilibration with 1× Equilibration Buffer (diluted from 5× stock with deionized water at 1:5) for 10–30 min at room temperature, excess buffer was gently removed. Subsequently, 50 μL TdT reaction mixture (prepared from ddH_2O, 5× Equilibration Buffer, FITC-12-dUTP labeling mix, and recombinant TdT

enzyme) was added to each section and incubated at 37°C for 60 min in the dark. For negative controls, the TdT enzyme was replaced with ddH_2O. Sections were then rinsed with PBS (5 min × 3, protected from light), counterstained with DAPI at 37°C for 10 min, and washed again with PBS. Finally, slides were mounted with buffered glycerol and examined under a fluorescence microscope.

2.7. Immunohistochemical analysis

Paraffin-embedded sections of diced cartilage grafts were subjected to immunohistochemical staining. Sections were deparaffinized in xylene (20 min × 3), rehydrated through graded ethanol (100%, 95%, 85%, and 75%, 5 min each), and rinsed in distilled water. Antigen retrieval was performed in 0.01 M citrate buffer (pH 6.0) by heating to boiling, followed by continuous heating for 20 min and natural cooling to room temperature. Sections were then washed in PBS (pH 7.2–7.6) three times (3 min each). Endogenous enzyme activity was blocked by incubation with 1% periodic acid for 10 min at room temperature, followed by PBS washing. Sections were incubated with appropriately diluted primary antibodies overnight at 4°C, rinsed with PBS (5 min × 3), and subsequently incubated with HRP-conjugated anti-rabbit IgG polymer secondary antibody (50–100 μL per section) at 37°C for 30 min. After PBS washing, color development was achieved using DAB working solution under microscopic monitoring (1–5 min), and the reaction was terminated by rinsing with distilled water. Sections were counterstained with hematoxylin for 5–10 min, blued in PBS, dehydrated through graded ethanol (60%–100%), cleared in xylene (10 min × 2), sealed with neutral resin, and observed under a light microscope.

2.8. Cell culture

Human immortalized chondrocytes (Cat. No. AW-CNH489) and human primary adipose-derived stem cells (hADSCs; Cat. No. AW-YCH027) were commercially purchased from Abiowell (Changsha, China). Human chondrocytes were cultured in human chondrocyte-specific medium (Abiowell, Cat. No. AW-MC018) supplemented with 10% fetal bovine serum (FBS) and 1% penicillin–streptomycin under standard conditions (37°C, 5% CO_2, saturated humidity). When cell confluence reached approximately 80%, cells were detached by trypsinization and passaged at a 1:2 split ratio. hADSCs were maintained in human ADSC-specific medium (Abiowell, Cat. No. AW-MC025) containing 10% FBS and 1% penicillin–streptomycin at 37°C in a humidified atmosphere with 5% CO_2. Cells were subcultured at ~ 80% confluence following trypsin digestion using the same 1:2 passaging protocol.

2.9. Cell viability assay

Cell viability was evaluated using a Cell Counting Kit-8 (CCK-8) assay. Logarithmically growing human chondrocytes were harvested, counted, and seeded into 96-well plates at a density of 5×10^3 cells per well, with three replicates per group. After cell attachment, hydrogen peroxide (H_2O_2) was diluted to the indicated working concentrations (0, 100, 200, and 400 μM) using complete culture medium. Cells were treated for 0, 12, 24, and 48 h under standard culture conditions. At each time point, 10 μL of CCK-8 reagent was added to each well and incubated for an additional 4 h at 37°C with 5% CO_2. The absorbance at 450 nm was measured using a microplate reader. Cell viability was calculated as: Cell viability (%) = (OD_treated − OD_blank) / (OD_control − OD_blank) × 100%.

2.10. Western blot analysis

Human chondrocytes were treated with H_2O_2 at 0, 25, 100, and 200 μM for 24 h. Total proteins were extracted using RIPA lysis buffer after washing cells with pre-cooled PBS. Cell lysates were collected by scraping, sonicated for 1.5 min, incubated on ice for 10 min, and centrifuged at 12,000 rpm for 15 min at 4°C. The supernatants were collected for subsequent analysis. Protein concentrations were determined using a BCA protein assay kit according to the manufacturer's instructions. Equal amounts of protein were mixed with 5× loading buffer, boiled for 5 min, and separated by SDS–PAGE using 10%–12% resolving gels and 4.8% stacking gels. Proteins were then transferred onto NC membranes at a constant current of 300 mA. Membranes were blocked with 5% non-fat milk in PBST for 90 min at room temperature and incubated overnight at 4°C with primary antibodies against NLRP3 (30109-1-AP, 1:6000, Proteintech), P62 (18420-1-AP, 1:10000, Proteintech), Beclin-1 (11306-1-AP, 1:1000, Proteintech), β-actin (66009-1-Ig, 1:10000, Proteintech), Caspase-1 (22915-1-AP, 1:6000, Proteintech), LC3 (14600-1-AP, 1:6000, Proteintech), and GSDMD (20770-1-AP, 1:12000, Proteintech). After washing with PBST, membranes were incubated with HRP-conjugated secondary antibodies for 90 min at room temperature. Protein bands were visualized using an enhanced chemiluminescence (ECL) detection system and captured with a gel imaging system.

2.11. Transwell co-culture assay

A Transwell co-culture system was established using 24-well plates. ADSCs were seeded in the lower chamber at a density of 1×10^4 cells per well and allowed to adhere. Transwell inserts were then placed into the wells, and treated chondrocytes were trypsinized and seeded into the upper chambers. Cells were co-cultured at 37°C in a humidified incubator with 5% CO_2 for 48 h. After incubation, non-migrated cells in the upper chamber were gently removed with a cotton swab following PBS washing. The migrated cells were fixed with 4% paraformaldehyde and stained with 0.1% crystal violet for 5 min. After thorough washing, images were captured under a light microscope.

2.12. Hoechst/PI staining

Chondrocyte death was assessed using Hoechst 33342/propidium iodide (PI) double staining. Cells were treated according to the grouping described above, washed once with PBS, and incubated with 1 mL staining buffer. Subsequently, 5 μL Hoechst 33342 and 5 μL PI staining solution were added to each sample. After gentle mixing, cells were incubated at 4°C for 30 min in the dark. Following three washes with PBS, stained cells were observed and imaged under a fluorescence microscope.

2.13. Quantitative real-time PCR (RT-qPCR) analysis

Total RNA was extracted from treated chondrocytes using TRIzol reagent according to the manufacturer's protocol. Briefly, cells were lysed in 1 mL TRIzol and incubated at room temperature for 5 min, followed by addition of 200 μL chloroform. After vigorous shaking (15 s) and incubation (3 min), samples were centrifuged at 12,000 rpm for 15 min at 4°C. The aqueous phase was transferred to an RNase-free tube, mixed with an equal volume of isopropanol, and incubated for 10 min at room

temperature. RNA was precipitated by centrifugation (12,000 rpm, 10 min, 4°C), washed with 75% ethanol, air-dried, and dissolved in 20–30 μL RNase-free water. RNA concentration and purity were determined by spectrophotometry (A260/A280 ratio). For reverse transcription, 50 pg–5 μg total RNA was reverse-transcribed into cDNA using a commercial reverse transcription kit in a 20 μL reaction system containing dNTP mix, primer mix, 5× RT buffer, DTT, and reverse transcriptase. The reaction conditions were 50°C for 50 min followed by 85°C for 5 min. The synthesized cDNA was either used immediately for qPCR or stored at − 20°C. Quantitative PCR was performed using a SYBR Green-based detection system on a real-time PCR instrument. Gene-specific primers were designed based on sequences obtained from the NCBI database and synthesized commercially. Each reaction (10 μL per well) was conducted in triplicate. The amplification program consisted of an initial denaturation at 95°C for 10 min, followed by 40 cycles of 95°C for 15 s and 60°C for 30 s. Melt curve analysis was performed from 60°C to 95°C to verify amplification specificity. Relative gene expression levels were calculated using the 2^−ΔΔCt method with GAPDH as the internal reference. The primer sequences used for amplification are detailed in Table S1.

2.14. Flow cytometric analysis of intracellular ROS

Intracellular reactive oxygen species (ROS) levels were measured using 2',7'-dichlorofluorescin diacetate (DCFH-DA) staining followed by flow cytometry, as previously described. Briefly, treated chondrocytes were harvested and resuspended to obtain a single-cell suspension. DCFH-DA stock solution (10 mM) was diluted 1:1000 in serum-free medium to achieve a final concentration of 10 μM. After removal of the culture medium, cells were incubated with an appropriate volume of diluted DCFH-DA to fully cover the cells and maintained at 37°C for 20 min in the dark. Following incubation, cells were washed three times with serum-free medium to remove excess probe, trypsinized, and collected by centrifugation. The fluorescence intensity of DCF was immediately analyzed using a flow cytometer, and data were processed to quantify intracellular ROS levels.

2.15. Enzyme-linked immunosorbent assay (ELISA)

Cell culture supernatants were collected and centrifuged at 1500 rpm for 5 min to remove cellular debris. The clarified supernatants were either immediately subjected to analysis or aliquoted and stored at − 80°C until further use. The concentrations of target proteins in the culture media were determined using enzyme-linked immunosorbent assay (ELISA) kits according to the manufacturer’s instructions. Absorbance was measured using a microplate reader, and protein concentrations were calculated based on the corresponding standard curves.

2.16. Statistical analysis

All statistical analyses were performed using GraphPad Prism. Quantitative data are presented as mean ± standard deviation (mean ± SD). Comparisons between two groups were conducted using the Student’s t-test, while differences among multiple groups were analyzed by one-way analysis of variance (one-way ANOVA). A P value < 0.05 was considered statistically significant.

2.17. Checklist statement

The work has been reported in line with the Additional file 1: ARRIVE guidelines 2.0.

3. Results and discussion

3.1. Construction and characterization of ADSC-derived cell sheets

Adipose tissue harvested from the rabbit inguinal region was subjected to enzymatic digestion and centrifugation, yielding a visible white cellular pellet at the bottom of the tube. Following resuspension and seeding, cells began to adhere within 4–6 h. By 24 h, adherent cells exhibited progressive spreading with a spindle-shaped morphology, strong refractive properties, and a relatively uniform appearance. After approximately 5 d of culture, confluence reached 70%–80%, and the cells displayed characteristic whirlpool- or bundle-like arrangements (Fig. 1a). Flow cytometric analysis confirmed the mesenchymal phenotype of the isolated cells. The positive expression rates of CD73, CD90, and CD105 were 98.15%, 97.49%, and 98.70%, respectively, whereas the hematopoietic markers CD34 and CD45 were minimally expressed at 2.37% and 0.62% (Fig. 1b). Upon culture in temperature-responsive dishes for 14 d, subsequent low-temperature treatment (~ 40 min) induced spontaneous detachment of an intact, white, membranous construct from the culture surface. The resulting adipose-derived stem cell (ADSC) sheet exhibited a smooth surface and robust mechanical integrity (Fig. 1c). Scanning electron microscopy further revealed densely aligned spindle-shaped cells interconnected by prominent cell–cell junctions, accompanied by abundant extracellular matrix deposition and indistinct cellular boundaries, indicative of a well-organized and cohesive cell sheet structure (Fig. 1d).

3.2. ADSC-derived cell sheets improve histological morphology and cell viability of diced cartilage grafts

Rabbit auricular cartilage was processed into 0.5–1.0 mm^3 particles and implanted subcutaneously on the dorsal side (Fig. 2a, b). Histological evaluation at 1, 3, and 6 months revealed distinct differences in graft preservation among treatments. At 1 month, ADSC sheet–wrapped grafts displayed fewer chondrocytes with nuclear loss compared with the other groups, and this protective effect persisted through 3 and 6 months. In contrast, the control group exhibited minimal temporal variation. Autologous fascia wrapping showed partial improvement at 6 months relative to 1 month, whereas ADSC sheet treatment maintained consistently lower levels of nuclear loss at both intermediate and late stages (Fig. 2c), indicating sustained cellular preservation. Type II collagen staining was primarily localized within the chondrocyte cytoplasm and surrounding extracellular matrix (Fig. 2d). Throughout the observation period, ADSC sheet–wrapped grafts demonstrated a greater proportion of type II collagen–positive areas than unwrapped grafts, with the strongest matrix retention observed in the ADSC sheet group, suggesting enhanced maintenance of cartilage-specific phenotype. Apoptotic cells, identified by TUNEL staining (Fig. 2e), were relatively abundant at 1 month across all groups but decreased over time. Notably, ADSC sheet treatment was consistently associated with fewer apoptotic cells at each time point, while autologous fascia wrapping conferred moderate protection compared with controls.

Between 3 and 6 months, apoptosis levels remained largely unchanged in the control group, whereas ADSC sheet treatment further reduced cell death at the later stage. Overall, both ADSC and autologous fascia wrapping mitigated chondrocyte loss within the grafts, with ADSC sheets providing superior long-term preservation of cellular viability and cartilage matrix integrity.

3.3. ADSC-derived cell sheets improve the microenvironment of diced cartilage grafts

Following implantation, diced cartilage grafts are exposed to ischemia, inflammatory infiltration, and metabolic stress, leading to excessive ROS accumulation and activation of the NLRP3 inflammasome, which in turn triggers chondrocyte pyroptosis and compromises graft viability. Autophagy acts as an adaptive protective mechanism in this microenvironment by mitigating oxidative stress and suppressing inflammasome activation, thereby preserving chondrocyte survival and cartilage matrix integrity [31]. Pyroptosis-related markers NLRP3, Caspase-1, and GSDMD were detectable in cartilage grafts at 1, 3, and 6 months, presenting as yellow-brown staining signals (Fig. 3a–c). Among the different interventions, ADSC sheet–wrapped grafts consistently exhibited the lowest expression levels, whereas autologous fascia wrapping produced a moderate reduction compared with unwrapped controls. Expression was generally higher at 1 month and declined thereafter. By 6 months, NLRP3 and GSDMD levels were similar to those at 3 months, while Caspase-1 expression in the ADSC sheet group showed a further decrease, suggesting sustained attenuation of inflammasome activity. Oxidative stress–associated proteins displayed coordinated changes. NOX4 and SOD1 were present at all examined time points (Fig. 3d, e). Membrane wrapping was accompanied by reduced NOX4 expression and enhanced SOD1 expression relative to unwrapped grafts, with the most pronounced modulation observed in the ADSC sheet group. Early-stage grafts were characterized by elevated NOX4 and relatively low SOD1 levels, whereas later stages exhibited decreased oxidative stress and partial restoration of antioxidant capacity. In particular, NOX4 expression in the ADSC sheet group declined further at 6 months compared with 3 months, while SOD1 levels remained relatively stable. Autophagy-related proteins LC3Ⅱ, Beclin-1, and P62 were detectable throughout the observation period, appearing as green fluorescence signals (Fig. 3f–h). ADSC sheet treatment was associated with enhanced LC3Ⅱ and Beclin-1 expression and reduced P62 accumulation compared with other groups, whereas autologous fascia wrapping showed intermediate effects. Temporal variations in these autophagy markers were modest. Overall, ADSC sheets appear to reshape the graft microenvironment by promoting autophagic activity while suppressing pyroptosis and oxidative stress, thereby contributing to improved preservation of cartilage tissue.

3.4. H_2O_2 induces pyroptosis and transcriptomic remodeling in chondrocytes

As a relatively stable and diffusible ROS, H_2O_2 serves as a key mediator of oxidative damage, disrupting chondrocyte redox homeostasis and contributing to cell death and matrix degradation in cartilage grafts [32]. Exposure of chondrocytes to increasing concentrations of H_2O_2 (0, 100, 200, and 400 μM) for 12, 24,

and 48 h resulted in a progressive decline in cell viability, with both dose and duration contributing to the inhibitory effect. At 12 and 24 h, viability decreased in a concentration-dependent manner, whereas a more pronounced reduction was observed at 48 h, particularly in the 400 μM group. Based on these kinetics, 100–200 μM H_2O_2 for 24 h was selected for subsequent experiments, with 100 μM providing a stable and reproducible injury condition (Fig. 4a). Consistent with the reduction in viability, TUNEL staining revealed a concentration-dependent increase in cell death after 24 h of H_2O_2 exposure. The 100 μM group exhibited a marked elevation in TUNEL-positive cells, while 200 μM produced a slightly attenuated yet still significantly higher level compared with controls (Fig. 4b). In parallel, pyroptosis-associated proteins, including GSDMD, Caspase-1, and NLRP3, were upregulated across 25–200 μM H_2O_2, with the most robust induction at 100 μM (Fig. 4c). Ultrastructural examination further illustrated these changes: whereas control chondrocytes displayed intact and smooth plasma membranes, cells treated with 100 μM H_2O_2 developed membrane blebbing, rupture, and cytoplasmic leakage—hallmarks of pyroptotic morphology (Fig. 4d). Together, these data establish a reliable oxidative stress–induced pyroptosis model in chondrocytes. To obtain a global view of the molecular alterations underlying H_2O_2-induced injury, RNA sequencing was performed to compare normal (CHSV) and injured (CH2) chondrocytes. A substantial number of differentially expressed genes were identified, with volcano plots indicating a balanced distribution of up- and downregulated transcripts (Fig. 4e). Principal component analysis and correlation heatmap confirmed high reproducibility within groups (Fig. 4f-g). Gene Ontology enrichment highlighted processes related to programmed cell death, cell death, regulation of acute inflammatory response, and apoptotic process (Fig. 4h). KEGG pathway analysis further revealed significant enrichment in “TNF signaling pathway”, “Autophagy – animal”, “mTOR signaling pathway”, and “IL-17 signaling pathway”, suggesting coordinated remodeling of autophagy and inflammatory signaling following oxidative injury (Fig. 4i).

3.5. ADSCs attenuate H_2O_2-induced chondrocyte pyroptosis and oxidative stress via autophagy regulation

Ultrastructural analysis by transmission electron microscopy further supported these molecular observations. Control chondrocytes exhibited intact cellular architecture and abundant organelles, including endoplasmic reticulum, mitochondria, and Golgi apparatus. In contrast, oxidatively injured cells showed disrupted structure and reduced organelle content. ADSC treatment markedly restored cellular integrity, accompanied by an increased number of autophagosomes (400–2000 nm) characterized by single- or double-membrane structures containing partially degraded material. Autophagosome formation was reduced in the model group, enhanced by ADSCs, further promoted by rapamycin (RAPA), and suppressed by bafilomycin A1 (Baf-A1) (Fig. 5a). At the transcriptional level, oxidative injury was associated with downregulation of LC3B and Beclin-1 and upregulation of P62. ADSC treatment reversed this pattern, increasing LC3B and Beclin-1 while decreasing P62 expression; RAPA amplified these changes, whereas Baf-A1 exerted the opposite effect (Fig. 5b–d). Protein analyses yielded consistent results, with restoration of the LC3Ⅱ/LC3Ⅰ ratio and Beclin-1 levels and reduction of P62 following ADSC intervention (Fig. 5e–h). These findings indicate that ADSCs reactivate autophagic flux in oxidatively stressed chondrocytes.

Functionally, oxidative stress impaired chondrocyte migration and viability, increased cell death, and elevated membrane permeability. ADSC treatment substantially improved migratory capacity and cell viability while reducing TUNEL- and PI-positive cells; these protective effects were potentiated by RAPA and attenuated by Baf-A1 (Fig. 6a–d). Molecular analyses further demonstrated that H_2O_2 injury upregulated NLRP3, Caspase-1, and GSDMD-N at both mRNA and protein levels. ADSCs suppressed the expression of these pyroptosis-related mediators, with RAPA enhancing and Baf-A1 reversing the inhibitory effect (Fig. 6e–k). Intracellular ROS accumulation followed a similar trend, being elevated in the model group, reduced by ADSCs, further decreased by RAPA, and increased by Baf-A1 (Fig. 6l). Biochemical assessment revealed increased malondialdehyde (MDA) and decreased superoxide dismutase (SOD) levels under oxidative stress, both of which were normalized by ADSC treatment in an autophagy-dependent manner, as evidenced by modulation with RAPA and Baf-A1 (Fig. 6m–n). In parallel, pro-inflammatory cytokines IL-1β, IL-18, and TNF-α were markedly elevated following H_2O_2 exposure, whereas ADSCs significantly suppressed their secretion, an effect strengthened by RAPA and weakened by Baf-A1 (Fig. 6o–q). Collectively, these findings demonstrate that ADSCs mitigate H_2O_2-induced pyroptosis, oxidative stress, and inflammatory responses in chondrocytes through restoration of autophagic activity, thereby conferring robust cytoprotective effects.

4. Conclusions

In summary, ADSC sheets significantly improve the survival and regeneration of transplanted cartilage by optimizing the graft microenvironment. Mechanistically, ADSC sheets inhibit activation of the NLRP3/Caspase-1/GSDMD signaling pathway, thereby suppressing chondrocyte pyroptosis and inflammatory injury. Meanwhile, ADSC sheets reduce oxidative stress and enhance autophagy, which together maintain cellular homeostasis and preserve chondrocyte viability, ultimately promoting cartilage regeneration. Compared with autologous perichondrium, ADSC sheet wrapping exhibits superior protective effects, likely due to the higher abundance of mesenchymal stem cells and the three-dimensional architecture that enhances paracrine signaling. Overall, ADSC sheets represent a promising biomimetic strategy for improving the stability and regenerative potential of diced cartilage grafts.

Declarations

Funding Declaration

This work was supported by the Hunan Provincial Natural Science Foundation (2023JJ30542), the Hunan Provincial Furong Talent Program, the Key Scientific Research Project of the Hunan Provincial Department of Education (25A0338), the Graduate Research and Innovation Project of University of South China (243YXC006), and the Xiangjiang Laboratory “Unveiling the List and Leading the Way” Project (25XJJB02).

Declaration of interests

The authors declare no conflicts of interest.

Ethics approval and consent to participate

The human immortalized chondrocytes (Cat. No. AW-CNH489) and human primary adipose-derived stem cells (Cat. No. AW-YCH027) used in this study were commercially obtained from Abiowell (Changsha, China). According to the supplier, all donor tissues were collected after written informed consent had been obtained from the donors or their legally authorized representatives, and tissue procurement complied with applicable ethical regulations. Since only commercially available, anonymized human cell products were used and no human participants were directly recruited by the authors, additional local institutional ethics approval was not required.

Animal Ethics declaration

The animal study was conducted under the project entitled "Study on VEGF membrane and ADSC sheet for improving the microenvironment of diced cartilage grafts by inhibiting chondrocyte pyroptosis" and was approved by the Experimental Animal Ethics Committee of the University of South China (Approval No. USC2021XS097; approval date: June 5, 2021). All animal procedures were performed in accordance with the institutional guidelines for the care and use of laboratory animals.

Use of Artificial Intelligence

During the preparation of this manuscript, the authors used DeepSeek solely to assist with English language editing and improve the readability of the text. The AI tool was not used to generate scientific content, perform data analysis, interpret results, or draw conclusions. All AI-assisted text was carefully reviewed, edited, and verified by the authors. The authors take full responsibility for the content of this manuscript.

CRediT authorship contribution statement

Junlin Liao and Jianda Zhou onceived the idea, initiated the project, and designed the experiments; Li Li, Yan Chen, and Tianjing Yu conducted the experiments and analyzed the data; Yi Wei drafted the manuscript; Zhengyang Li, Can Liu, and Wencan Li reviewed and edited the manuscript; All authors have seen and approved the final version.

Data availability

Data will be made available on request.

References

1. Hudise, J. Y., Aldhabaan, S. A. & Aldosari, B. F. Complications of the nasal dorsum reconstruction using autologous or alloplastic grafts: evidence from systematic review and meta-analysis. *Braz J Otorhinolaryngol* **88**, 406-420, doi:10.1016/j.bjorl.2020.07.001 (2022).

2. Erol, O. O. Injection of Compressed Diced Cartilage in the Correction of Secondary and Primary Rhinoplasty: A New Technique with 12 Years' Experience. *Plast Reconstr Surg* **140**, 673e-685e, doi:10.1097/prs.0000000000003815 (2017).
3. Xiang, X., Wang, X. & Wang, S. The Treatment of Alar Base Depression in Rhinoplasty with Diced Autologous Cartilage or Mass Cartilage: A Systematic Review. *Aesthetic Plast Surg* **48**, 3779-3789, doi:10.1007/s00266-024-04008-y (2024).
4. Peer, L. A. The neglected septal cartilage graft, with experimental observations on the growth of human cartilage grafts. *Arch Otolaryngol (1925)* **42**, 384-396, doi:10.1001/archotol.1945.00680040504008 (1945).
5. Kim, S. H., Suh, J. H. & Jang, Y. J. Histomorphological Findings of Cartilage and Surrounding Tissues According to Thickness and Manipulations in Rabbits. *Aesthet Surg J* **42**, Np489-np500, doi:10.1093/asj/sjac028 (2022).
6. Dong, W., Wang, X., Zhao, Z. & Fan, F. Viability and Stability of Various-Sized Free Diced Cartilage in an Experimental Study. *Aesthet Surg J* **43**, Np143-np154, doi:10.1093/asj/sjac263 (2023).
7. Chen, H., Wang, X. & Deng, Y. Complications Associated with Autologous Costal Cartilage Used in Rhinoplasty: An Updated Meta-Analysis. *Aesthetic Plast Surg* **47**, 304-312, doi:10.1007/s00266-022-03075-3 (2023).
8. Kemaloğlu, C. A. & Tekin, Y. A comparison of diced cartilage grafts wrapped in perichondrium versus fascia. *Aesthetic Plast Surg* **38**, 1164-1168, doi:10.1007/s00266-014-0403-6 (2014).
9. Landa, M., Ninchritz, E., Álvarez, L., Palicio, I. & Urreta, I. Autologous Tragal Perichondrium Graft for Vocal Fold Scar and Sulcus Vocalis. *J Voice* **36**, 701-706, doi:10.1016/j.jvoice.2020.08.024 (2022).
10. Takao, T. *et al.* A novel chondrocyte sheet fabrication using human-induced pluripotent stem cell-derived expandable limb-bud mesenchymal cells. *Stem Cell Res Ther* **14**, 34, doi:10.1186/s13287-023-03252-4 (2023).
11. Jia, W., He, W., Wang, G., Goldman, J. & Zhao, F. Enhancement of Lymphangiogenesis by Human Mesenchymal Stem Cell Sheet. *Adv Healthc Mater* **11**, e2200464, doi:10.1002/adhm.202200464 (2022).
12. Oie, Y. *et al.* Clinical Trial of Autologous Cultivated Limbal Epithelial Cell Sheet Transplantation for Patients with Limbal Stem Cell Deficiency. *Ophthalmology* **130**, 608-614, doi:10.1016/j.ophtha.2023.01.016 (2023).
13. Ramakrishnan, V. M. & Boyd, N. L. The Adipose Stromal Vascular Fraction as a Complex Cellular Source for Tissue Engineering Applications. *Tissue Eng Part B Rev* **24**, 289-299, doi:10.1089/ten.TEB.2017.0061 (2018).
14. Orbay, H., Tobita, M., Hyakusoku, H. & Mizuno, H. Effects of adipose-derived stem cells on improving the viability of diced cartilage grafts. *Plast Reconstr Surg* **129**, 369-377, doi:10.1097/PRS.0b013e31822b65fd (2012).
15. Yin, H. *et al.* Effect of Stromal Vascular Fractions on Angiogenesis of Injected Diced Cartilage. *J Craniofac Surg* **33**, 713-718, doi:10.1097/scs.0000000000007996 (2022).

16. Yao, S., Li, Y., Ruan, H., Wu, L. & Zeng, H. Gubi Decoction Ameliorates Porous Cartilage Endplate in an Intervertebral Disc Degeneration Model Mouse Through Inhibition of NF-κB Activity and Pyroptosis. *J Inflamm Res* **18**, 5293-5309, doi:10.2147/jir.S492365 (2025).
17. Wu, X. *et al.* Therapeutic potential of quercitrin in intervertebral disc degeneration: Targeting pyroptosis and inflammation. *Int Immunopharmacol* **156**, 114680, doi:10.1016/j.intimp.2025.114680 (2025).
18. Broz, P. Pyroptosis: molecular mechanisms and roles in disease. *Cell Res* **35**, 334-344, doi:10.1038/s41422-025-01107-6 (2025).
19. Gong, Y. *et al.* Maltol ameliorates intervertebral disc degeneration through inhibiting PI3K/AKT/NF-κB pathway and regulating NLRP3 inflammasome-mediated pyroptosis. *Inflammopharmacology* **31**, 369-384, doi:10.1007/s10787-022-01098-5 (2023).
20. Zhao, K. *et al.* Acid-sensing ion channels regulate nucleus pulposus cell inflammation and pyroptosis via the NLRP3 inflammasome in intervertebral disc degeneration. *Cell Prolif* **54**, e12941, doi:10.1111/cpr.12941 (2021).
21. Ebata, T. *et al.* Noncanonical Pyroptosis Triggered by Macrophage-Derived Extracellular Vesicles in Chondrocytes Leading to Cartilage Catabolism in Osteoarthritis. *Arthritis Rheumatol* **75**, 1358-1369, doi:10.1002/art.42505 (2023).
22. Zu, Y., Mu, Y., Li, Q., Zhang, S. T. & Yan, H. J. Icariin alleviates osteoarthritis by inhibiting NLRP3-mediated pyroptosis. *J Orthop Surg Res* **14**, 307, doi:10.1186/s13018-019-1307-6 (2019).
23. Shi, W. *et al.* Dynamic hyaluronic acid hydrogel with covalent linked gelatin as an anti-oxidative bioink for cartilage tissue engineering. *Biofabrication* **14**, doi:10.1088/1758-5090/ac42de (2021).
24. Li, H. *et al.* Reprogramming Macrophage Polarization, Depleting ROS by Astaxanthin and Thioketal-Containing Polymers Delivering Rapamycin for Osteoarthritis Treatment. *Adv Sci (Weinh)* **11**, e2305363, doi:10.1002/advs.202305363 (2024).
25. Clarke, A. J. & Simon, A. K. Autophagy in the renewal, differentiation and homeostasis of immune cells. *Nat Rev Immunol* **19**, 170-183, doi:10.1038/s41577-018-0095-2 (2019).
26. Li, W. *et al.* Selective autophagy of intracellular organelles: recent research advances. *Theranostics* **11**, 222-256, doi:10.7150/thno.49860 (2021).
27. Gao, W., Wang, X., Zhou, Y., Wang, X. & Yu, Y. Autophagy, ferroptosis, pyroptosis, and necroptosis in tumor immunotherapy. *Signal Transduct Target Ther* **7**, 196, doi:10.1038/s41392-022-01046-3 (2022).
28. Liao, K. *et al.* KCNK5 Regulating Potassium Efflux and Inducing Pyroptosis in Corneal Epithelial Cells Through TNFSF10-Mediated Autophagy in Dry Eye. *Invest Ophthalmol Vis Sci* **65**, 34, doi:10.1167/iovs.65.1.34 (2024).
29. Wu, D. *et al.* PPAR γ activation in chondrocytes alleviates glucocorticoid-induced oxidative stress, mitochondrial impairment, and pyroptosis via autophagic flow enhancement. *Chem Biol Interact* **390**, 110877, doi:10.1016/j.cbi.2024.110877 (2024).

30. Xu, L. *et al.* Attenuation of experimental osteoarthritis with human adipose-derived mesenchymal stem cell therapy: inhibition of the pyroptosis in chondrocytes. *Inflamm Res* **72**, 89-105, doi:10.1007/s00011-022-01655-2 (2023).
31. Xu, K. *et al.* SIRT3 ameliorates osteoarthritis via regulating chondrocyte autophagy and apoptosis through the PI3K/Akt/mTOR pathway. *Int J Biol Macromol* **175**, 351-360, doi:10.1016/j.ijbiomac.2021.02.029 (2021).
32. Collins, J. A. *et al.* Sirtuin 6 (SIRT6) regulates redox homeostasis and signaling events in human articular chondrocytes. *Free Radic Biol Med* **166**, 90-103, doi:10.1016/j.freeradbiomed.2021.01.054 (2021).

Figures

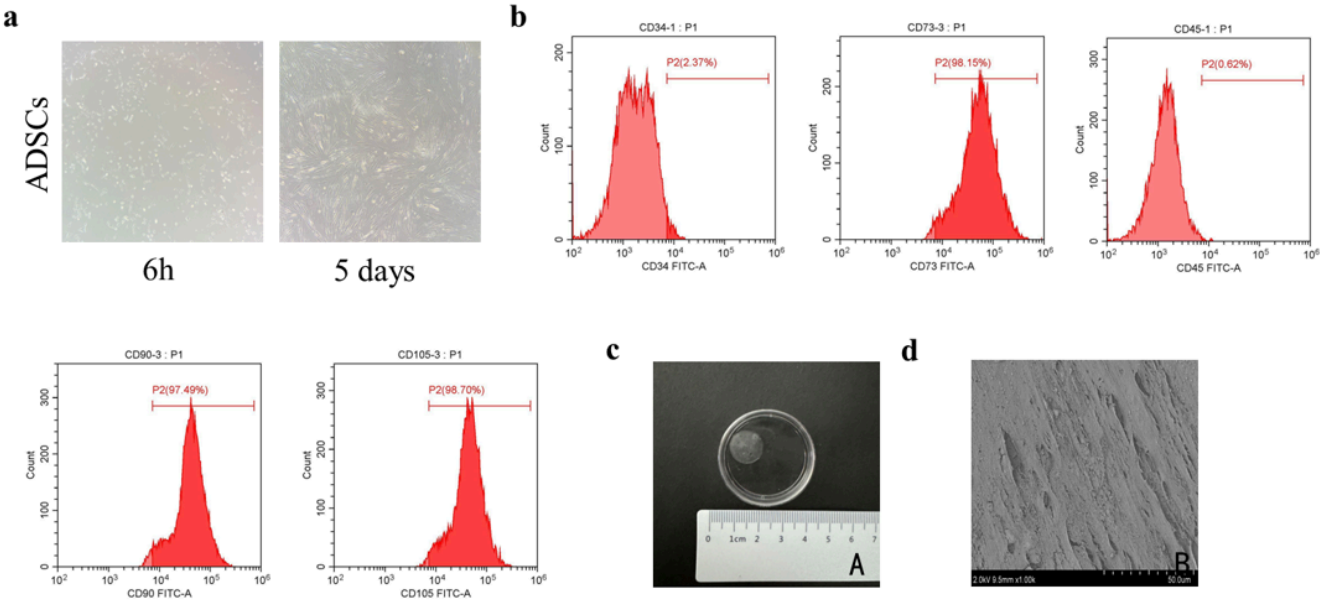


Figure 1

Isolation, identification, and sheet formation of adipose-derived stem cells (ADSCs).

(a) Morphological characteristics of ADSCs isolated from rabbit inguinal adipose tissue. After enzymatic digestion and centrifugation, cells were seeded and adhered within 4–6 h. At 24 h, adherent cells exhibited spindle-shaped morphology with strong refractive properties. After approximately 5 d of culture, cells reached 70%–80% confluence and displayed typical whirlpool- or bundle-like growth patterns. (b) Flow cytometric analysis of surface markers confirming the mesenchymal phenotype of ADSCs, showing high expression of CD73, CD90, and CD105, and minimal expression of hematopoietic markers CD34 and CD45. (c) Macroscopic appearance of the ADSC sheet formed on temperature-responsive culture dishes after 14 d of culture and low-temperature treatment, showing an intact, white membranous structure with good mechanical integrity. (d) Scanning electron microscopy (SEM) image of the ADSC sheet revealing densely aligned spindle-shaped cells interconnected by cell–cell junctions

and embedded within abundant extracellular matrix, forming a cohesive and well-organized cell sheet architecture.

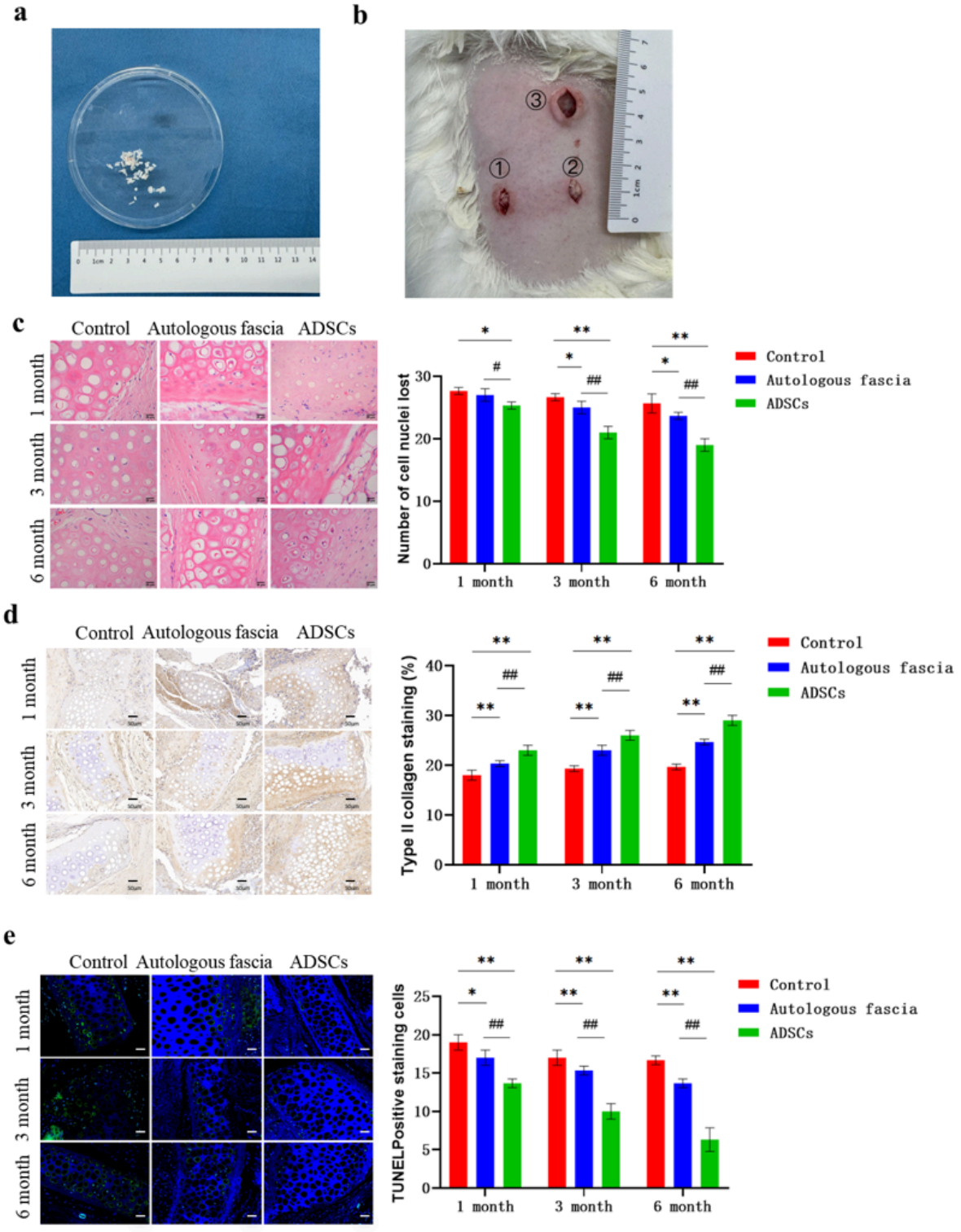


Figure 2

ADSC sheet wrapping enhances long-term preservation of implanted cartilage particles in vivo.

(a) Schematic illustration of the preparation and subcutaneous implantation of rabbit auricular cartilage particles (0.5–1.0 mm^3) on the dorsal side. (b) Representative images of the cartilage particle implantation procedure. (c) Histological analysis of chondrocyte nuclear loss in cartilage grafts at 1, 3, and 6 months post-implantation. ADSC sheet–wrapped grafts exhibited markedly fewer chondrocytes with nuclear loss compared with the control and autologous fascia groups, indicating improved cellular preservation. (d) Immunohistochemical staining of type II collagen showing its distribution within the chondrocyte cytoplasm and surrounding extracellular matrix. ADSC sheet–wrapped grafts displayed a higher proportion of type II collagen–positive areas, suggesting enhanced maintenance of the cartilage-specific extracellular matrix. (e) TUNEL staining for detection of apoptotic cells in cartilage grafts at different time points. Scale bar: 50 μm. $^{*}P < 0.05$, $^{**}P < 0.01$, $^{\#}P < 0.05$, $^{\#\#}P < 0.01$.

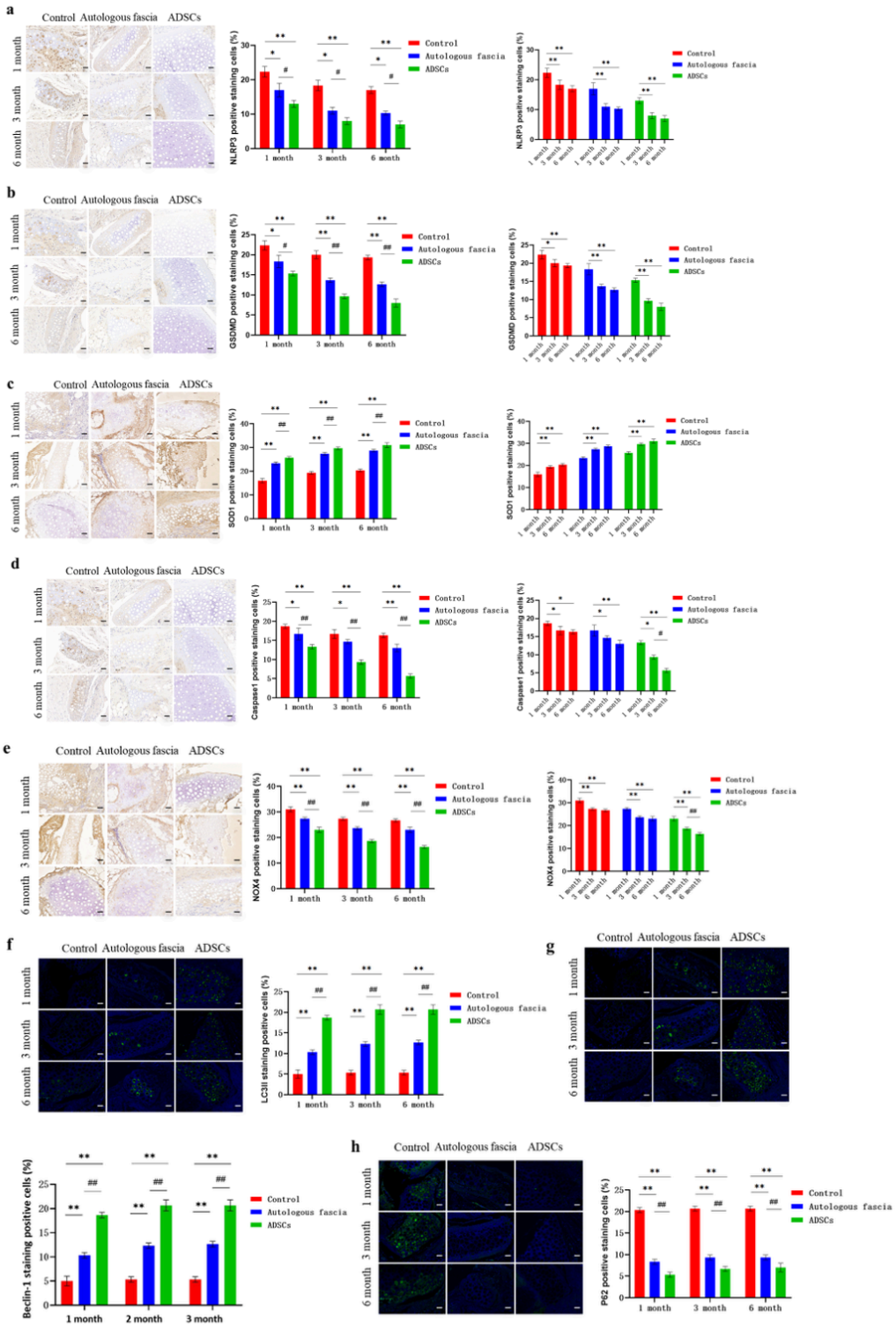


Figure 3

ADSC-derived cell sheets improve the microenvironment of diced cartilage grafts by regulating pyroptosis, oxidative stress, and autophagy.

(a–c) Immunohistochemical staining of pyroptosis-related proteins NLRP3, Caspase-1, and GSDMD in cartilage grafts at 1, 3, and 6 months post-implantation. Yellow-brown signals indicate positive

expression. ADSC sheet–wrapped grafts exhibited the lowest expression levels of these inflammasome-related markers compared with the control and autologous fascia groups, indicating suppression of pyroptosis. (d, e) Immunohistochemical analysis of oxidative stress–related proteins NOX4 and SOD1. Membrane wrapping reduced NOX4 expression and increased SOD1 expression relative to unwrapped grafts, with the most pronounced modulation observed in the ADSC sheet group. (f–h) Immunofluorescence staining of autophagy-related proteins LC3Ⅱ, Beclin-1, and P62 (green). ADSC sheet treatment increased LC3Ⅱ and Beclin-1 expression while reducing P62 accumulation, indicating enhanced autophagic activity. Scale bar: 50 μm. *$P < 0.05$, **$P < 0.01$, $^{\#}P < 0.05$, $^{\#\#}P < 0.01$.

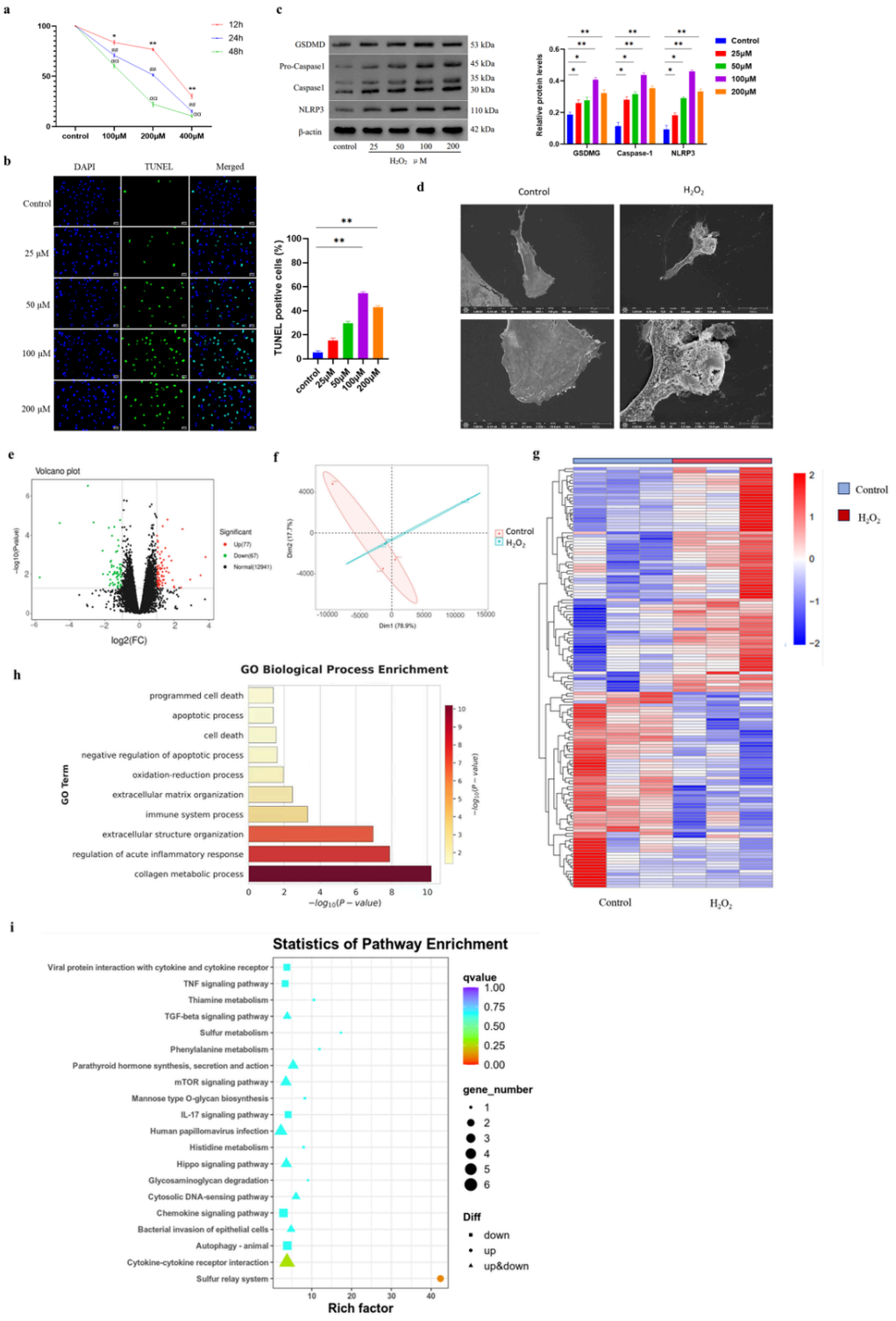


Figure 4

H_2O_2 induces pyroptosis and transcriptomic remodeling in chondrocytes.

(a) Cell viability of chondrocytes exposed to increasing concentrations of H_2O_2 (0, 100, 200, 400 μM) for 12, 24, and 48 h, showing dose- and time-dependent reductions. Based on these results, 100–200 μM H_2O_2 for 24 h was selected for subsequent experiments. (b) TUNEL staining of chondrocytes after 24 h

H_2O_2 exposure, demonstrating concentration-dependent increases in cell death, with marked elevation in the 100 μM group. (c) Western blot analysis of pyroptosis-associated proteins GSDMD, Caspase-1, and NLRP3, showing upregulation upon H_2O_2 treatment, most prominently at 100 μM. (d) Transmission electron microscopy images illustrating ultrastructural features of pyroptosis in chondrocytes exposed to 100 μM H_2O_2, including membrane blebbing, rupture, and cytoplasmic leakage, compared with intact membranes in control cells. (e) Volcano plot of differentially expressed genes (DEGs) between normal (CHSV) and H_2O_2-injured (CH2) chondrocytes. (f) Principal component analysis (PCA) showing distinct transcriptomic profiles between CHSV and CH2 groups. (g) The heatmap demonstrating the significant differences in mRNA expression between the two groups. (h) Gene Ontology (GO) enrichment analysis highlighting biological processes associated with apoptosis, cell death, and Inflammatory response. (i) KEGG pathway analysis revealing significant enrichment in in H_2O_2-injured chondrocytes. *P< 0.05, **P < 0.01.

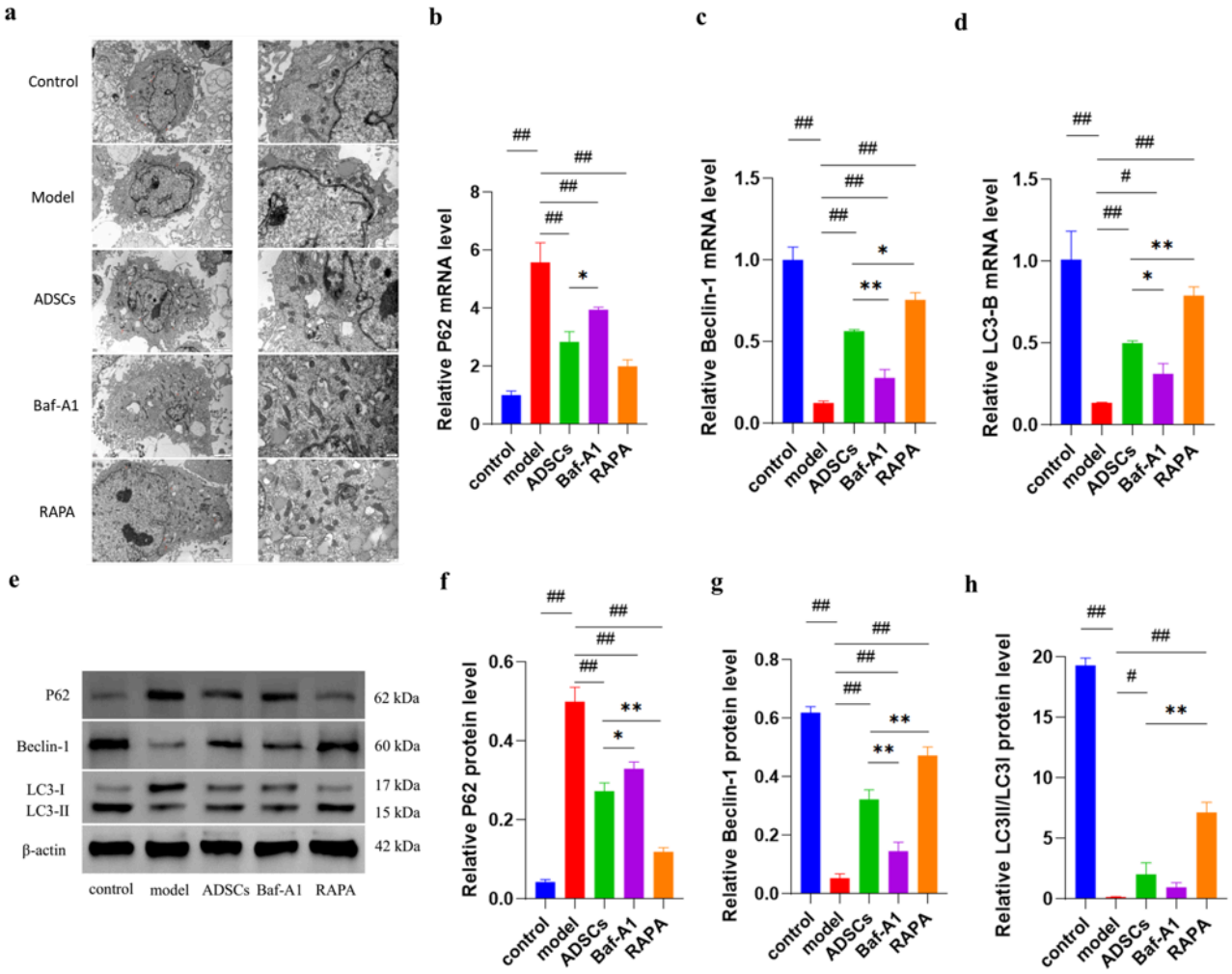


Figure 5

ADSCs restore autophagic flux in oxidatively injured chondrocytes.

(a) Transmission electron microscopy images showing ultrastructural features of chondrocytes. Control cells exhibited intact architecture with abundant organelles, whereas H_2O_2-treated cells displayed disrupted structure and reduced organelle content. ADSC treatment restored cellular integrity and increased autophagosome formation (400–2000 nm, single- or double-membrane structures). Autophagosome abundance was further enhanced by rapamycin (RAPA) and reduced by bafilomycin A1 (Baf-A1). (b–d) RT-qPCR analysis of autophagy-related genes LC3B, Beclin-1, and P62. ADSCs upregulated LC3B and Beclin-1 while downregulating P62; RAPA amplified, and Baf-A1 suppressed these effects. (e–h) Western blot analysis confirming restoration of autophagic proteins, including LC3Ⅱ/LC3Ⅰ ratio, Beclin-1, and decreased P62 following ADSC treatment. $^{*}P < 0.05$, $^{**}P < 0.01$, $^{\#}P < 0.05$, $^{\#\#}P < 0.01$.

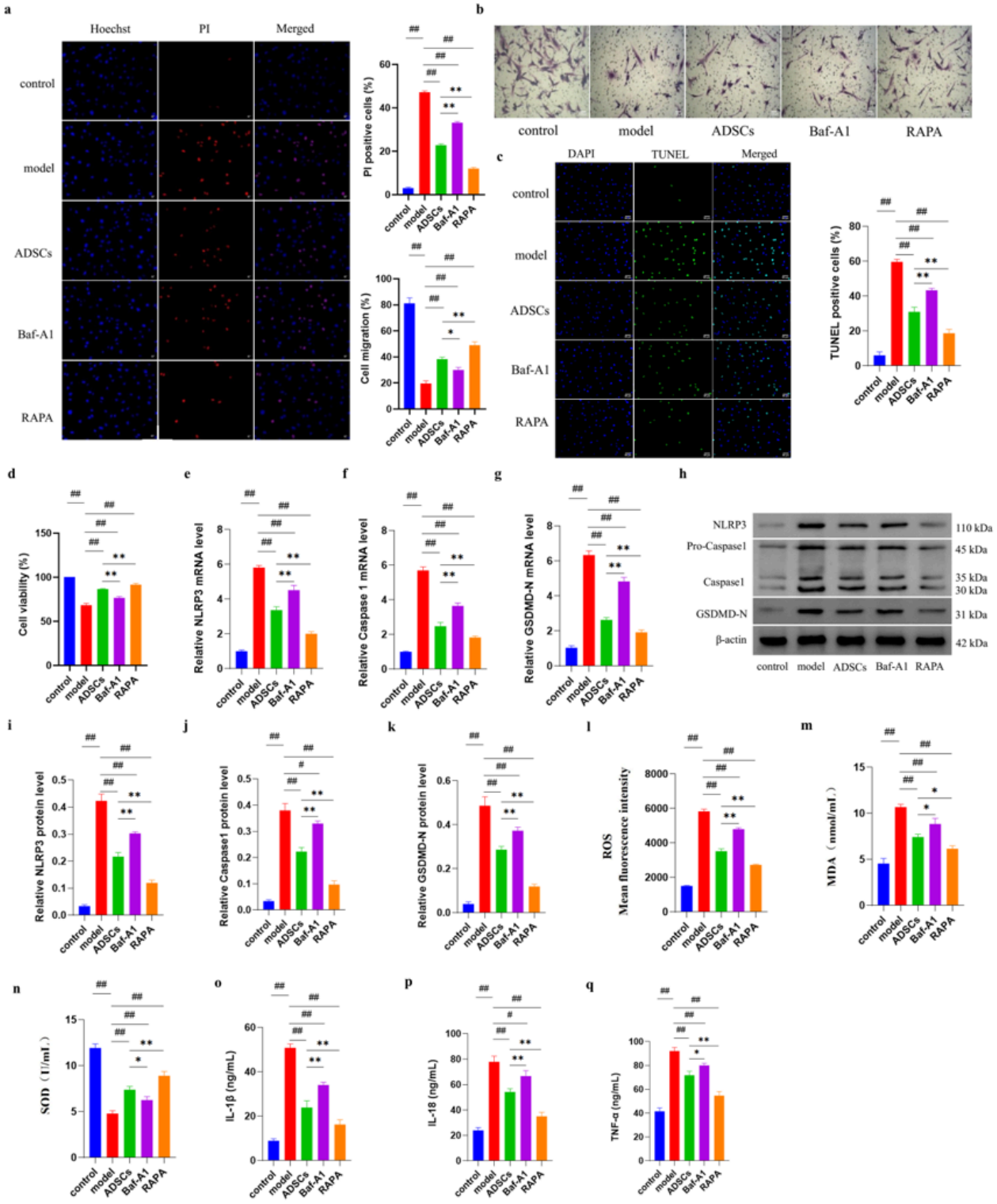


Figure 6

ADSCs mitigate oxidative stress, pyroptosis, and inflammation in chondrocytes through autophagy.

(a–d) Functional assays showing that oxidative stress impaired chondrocyte migration and viability and increased TUNEL- and PI-positive cell percentages. ADSC treatment restored migration and viability while reducing cell death, effects potentiated by RAPA and reversed by Baf-A1. (e–k) RT-qPCR and

Western blot analyses of pyroptosis-related mediators NLRP3, Caspase-1, and GSDMD-N. ADSCs suppressed their expression, with modulation by RAPA and Baf-A1 confirming autophagy dependence. (l) Intracellular ROS levels measured by fluorescence, showing reduction by ADSCs and further modulation by autophagy regulators. (m–n) Biochemical assays of malondialdehyde (MDA) and superoxide dismutase (SOD) levels, demonstrating normalization by ADSCs in an autophagy-dependent manner. (o–q) ELISA quantification of pro-inflammatory cytokines IL-1β, IL-18, and TNF-α, showing significant suppression by ADSCs, further enhanced by RAPA and attenuated by Baf-A1. *P < 0.05, **P < 0.01, $^{\#}$P < 0.05, $^{\#\#}P$ < 0.01.

Supplementary Files

This is a list of supplementary files associated with this preprint. Click to download.

- SupplementaryFigure.docx